Magnetic Properties and Structural Evolution in $Nd_{0.5}Sr_{1.5}MnO_4$

Chang Seop Hong,† Eun Ok Chi,† Wan Seop Kim,† Nam Hwi Hur,*,†
Kyu Won Lee,‡ and Chang Hee Lee§

Center for CMR Materials and Superconductivity Laboratory, Korea Research Institute of Standards and Science, Yusong, P.O. Box 102, Taejon 305-600, Korea, and Neutron Physics Department, HANARO Center, Korean Atomic Energy Research Institute, Yusong, P.O. Box 105, Taejon 305-600, Korea

Received August 31, 2000. Revised Manuscript Received November 27, 2000

The structural properties of single crystals of $R_{0.5}Sr_{1.5}MnO_4$ (R = La, Pr, and Nd) grown by the floating zone method have been studied using the neutron diffraction technique. In particular, the structure and its correlation with the magnetic properties have been investigated for $Nd_{0.5}Sr_{1.5}MnO_4$ by using both the neutron diffraction technique and the magnetization measurement as a function of temperature. An antiferromagnetic ordering appears to develop at about 130 K in the magnetization data, which coincides with the superlattice peaks shown in the neutron powder diffraction patterns below this temperature. The enhancement of the magnetization below 21 K is likely to be associated with the spin glasslike ordering of the Nd cations. With decreasing temperature, the axial Mn−O(2) bond distance shortens abruptly at the critical temperatures, accompanied by reducing the Jahn−Teller distortion. This behavior is evident that the magnetic transitions in $Nd_{0.5}Sr_{1.5}MnO_4$ are strongly correlated with the structural variations.

Introduction

There has been considerable interest in perovskite manganites, which is mainly due to the colossal magnetoresistance (CMR) characteristic found in these materials.[1] It has been known that the interplay among spin, charge, and lattice degrees of freedom is crucial to understand this fascinating phenomenon.[2,3] The competing interaction between them has thus been issued in the layered manganite as well as the perovskite one. The $n = 2$ member of the Ruddlesden−Popper phases, $A_{n+1}Mn_nO_{3n+1}$ (A = rare earth or alkaline earth), where $[MnO_6]$ octahedra are separated by an intervening rock-salt layer [AO] has offered a unique opportunity to explore the magneto transport behaviors in reduced dimensions.[4,5] As found in the perovskite phase,[6−9] the metal−insulator transition accompanied by the ferromagnetic ordering in the $n = 2$ phase is realized in the given doping range.[10,11] In contrast to this, the $n = 1$ phase exhibits an insulating state with competing ferromagnetic and antiferromagnetic interactions in the whole doping range.[12,13] These results reveal that the magnetic and transport properties of the manganites are quite sensitive to the dimensionality.

Among the $n = 1$ phases, $La_{1-x}Sr_{1+x}MnO_4$ has been extensively investigated by several groups. In particular, the $x = 0.5$ composition in which Mn^{3+} and Mn^{4+} exist as an equal ratio was focused due to its unique physical phenomena such as charge/orbital ordering and spin ordering. Elastic neutron scattering[14] and synchrotron X-ray diffraction were employed to reveal the ordering behaviors.[15] The melting of charge/orbital ordering in the same doping level was achieved by applying pulsed magnetic fields up to 40 T.[16] Despite extensive work on the $La_{1-x}Sr_{1+x}MnO_4$ system, relatively little is understood on other isostructural congeners which contain magnetic rare-earth ions.[17] We

* E-mail: nhhur@kriss.re.kr.
† Center for CMR Materials.
‡ Superconductivity Laboratory.
§ Korean Atomic Energy Research Institute.

(1) Jin, S.; Tiefel, T. H.; McCormack, M.; Fastnacht, R. A.; Ramesh, R.; Chel, H. *Science* **1994**, *264*, 413.
(2) Endoh, Y.; Hirota, K.; Ishihara, S.; Pkamoto, S.; Murakami, Y.; Nishizawa, A.; Fukuda, T.; Kimura, H.; Nojiri, H.; Kaneko, K.; Maekawa, S. *Phys. Rev. Lett.* **1999**, *82*, 4328.
(3) Uhlenbruck, S.; Teipen, R.; Klingeler, R.; Büchner, B.; Friedt, O.; Hücker, Kierspel, M.; H.; Niemöller, T.; Pinsard, L.; Revcolevschi, A.; Gross, R. *Phys. Rev. Lett.* **1999**, *82*, 185.
(4) Okuda, T.; Kimura, T.; Tokura, Y. *Phys. Rev.* **1999**, *B60*, 3370.
(5) Witte, N. S.; Goodman, P.; Lincoln, F. J.; March, R. H.; Kennedy, S. J. *Appl. Phys. Lett.* **1998**, *72*, 853.
(6) Urushibara, A.; Moritomo, Y.; Arima, T.; Asamitsu, A.; Kido, G.; Tokura, Y. *Phys. Rev.* **1995**, *B51*, 14103.
(7) Attfield, J. P. *Chem. Mater.* **1998**, *10*, 3239.
(8) Rao, C. N. R.; Arulraj, A.; Santosh, P. N.; Cheetham, A. K. *Chem. Mater.* **1998**, *10*, 2714.
(9) Hong, C. S.; Kim, W. S.; Chi, E. O.; Lee, K. W.; Hur, N. H. *Chem. Mater.* **2000**, *12*, 3509.
(10) Hur, N. H.; Kim, J.-T.; Yoo, K. H.; Park, Y. K.; Park, J.-C.; Chi, E. O.; Kwon, Y. U. *Phys. Rev.* **1998**, *B57*, 10740.
(11) Chi, E. O.; Kwon, Y.-U.; Kim, J.-T.; Hur, N. H. *Solid State Commun.* **1999**, *110*, 569.
(12) Moritomo, Y.; Tomioka, Y.; Asamitsu, A.; Tokura, Y. *Phys. Rev.* **1995**, *B51*, 3297.
(13) Bao, W.; Chen, C. H.; Carter, S. A.; Cheong, S.-W. *Solid State Commun.* **1996**, *98*, 55.
(14) Sternlieb, B. J.; Hill, J. P.; Wildgruber, U. C.; Luke, G. M.; Nachumi, B.; Moritomo, Y.; Tokura, Y. *Phys. Rev. Lett.* **1996**, *76*, 2169.
(15) Murakami, Y.; Kawada, H.; Kawata, H.; Tanaka, M.; Arima, T.; Moritomo, Y.; Tokura, Y. *Phys. Rev. Lett.* **1998**, *80*, 1932.
(16) Tokunaga, M.; Miura, N.; Moritomo, Y.; Tokura, Y. *Phys. Rev.* **1999**, *B59*, 11151.

10.1021/cm000702n CCC: $20.00
Published on Web 01/30/2001

have thus investigated the magnetic and structural properties of $R_{0.5}Sr_{1.5}MnO_4$ (R = La, Pr, and Nd), where single crystals are grown by the floating zone method. In this report, we mainly deal with the temperature-dependent magnetization and structural changes of $Nd_{0.5}Sr_{1.5}MnO_4$ and compare its properties with those of $La_{0.5}Sr_{1.5}MnO_4$ and $Pr_{0.5}Sr_{1.5}MnO_4$. An important finding is that the onset of the magnetic ordering directly reflects the structural change, suggestive of strong correlation between magnetism and structure.

Experimental Section

Single crystals of $R_{0.5}Sr_{1.5}MnO_4$ (R = La, Pr, and Nd) were grown by the floating zone method. Polycrystalline powders for the crystal growth were prepared using the solid-state reaction technique described below. Stoichiometric mixtures of corresponding rare-earth oxide, $SrCO_3$, and MnO_2 were calcined at 1000 °C for 12 h in air. The calcined sample was ground, pelletized, and sintered at 1300 °C for 48 h. The pressed rod which has a cylindrical shape (6 mm × 80 mm = diameter × length) was prepared from the cold-pressing of ground powders with a pressure of 200 MPa. The rod was annealed at 1450 °C for 20 h in air to be hardened. The sintered rod was cut into two pieces, which are used as seed and feed rods. The seed rod is fixed to the ceramic holder using platinum wire. The feed rod is hung with the platinum hook of the upper shaft inside the optical furnace. The furnace (Crystal Systems Inc.) is equipped with four mirrors and four halogen lamps with total input power of 4 kW. Both feed and seed rods are coaxially rotated in opposite directions at a rate of 25 rpm. The growth and oxygen flowing rates are 13 mm/h and 3 L/min, respectively. The temperature of the molten zone was measured by detecting blackbody radiation of graphite rod with a pyrometer. The temperatures of the focused area for $R_{0.5}Sr_{1.5}MnO_4$ samples are 1850 °C for Nd, 1860 °C for Pr, and 1900 °C for La. The temperature at the position of 6 mm below from the center is about 100 °C lower.

Electron-probe microanalysis (EPMA) was employed to estimate compositions of all crystals, revealing that nominal values are maintained in the crystals. The X-ray diffraction data were recorded in the angular range $10 \le 2\theta \le 120$ with a step size of 0.02 using a Rigaku RAD diffractometer equipped with Cu Kα radiation. Neutron diffraction data were measured over the 2θ range of 0−160 with a step size of 0.05 on a HRPD (high-resolution powder diffractometer), where a neutron source with $\lambda = 1.8348$ Å supplied by Ge(331) single-crystal monochromator was used at HANARO Center, KAERI, Korea. The ground crystalline samples were loaded in a vanadium can (Φ =12 mm, length = 45−55 mm) that is placed in the helium-filled Al shield for variable-temperature experiments. The diffraction data were analyzed by profile analysis based on the *Fullprof* program.[18] Six background parameters of Chebyshev polynomial, pseudo-Voigt peak shape function, and asymmetry parameters were included in the refinement process. The magnetic measurements were performed in the temperature range from 5 to 360 K using a Quantum Design MPMS-5 SQUID magnetometer and a PPMS-7 magnetometer.

Results and Discussion

Single crystals of $R_{0.5}Sr_{1.5}MnO_4$ (R = La, Pr, and Nd) grown from the floating zone technique were easily cleaved in the longitudinal direction due to their anisotropic nature. The XRD patterns of the cleaved surface show (00*l*) peaks only, indicating that the surface lies in the *ab* plane. Detailed structures of $R_{0.5}Sr_{1.5}MnO_4$ were analyzed with the neutron diffraction data that was collected with ground single crystal. Figure 1 displays the observed neutron diffraction data at 300 K, along with the theoretical diffraction patterns, of $Nd_{0.5}Sr_{1.5}MnO_4$. The initial structural model to be refined with the Rietveld profile analysis is based on the $n = 1$ member of the Ruddlesden−Popper phase which is known as the K_2NiF_4 type structure. All of the observed peaks in $Nd_{0.5}Sr_{1.5}MnO_4$ satisfied the reflection conditions of the space group $I4/mmm$, $h + k + l =$ even; $hk0$, $h + k =$ even; and $00l$, $l =$ even. Refinement with this model yields a satisfactory fit to the overall profile with the reliability factors of $R_p = 4.58\%$, $R_{wp} = 5.87\%$, and $\chi^2 = 2.32$. The space group is valid through the entire temperature, having parameters of $R_p = 3.98\%$, $R_{wp} = 5.13\%$, $\chi^2 = 3.5$ at 130 K, $R_p = 3.95\%$, $R_{wp} = 5.2\%$, $\chi^2 = 3.49$ at 21 K, and $R_p = 4.07\%$, $R_{wp} = 5.34\%$, $\chi^2 = 3.67$ at 10 K. The structures of $La_{0.5}Sr_{1.5}MnO_4$ and $Pr_{0.5}Sr_{1.5}MnO_4$ are virtually identical with that of $Nd_{0.5}Sr_{1.5}MnO_4$ and refined in a similar manner. Their structural parameters from neutron powder diffraction data at temperatures of 10 and 300 K for the samples are tabulated in Table 1. As can be seen in Figure 2, all of the structural parameters of $R_{0.5}Sr_{1.5}MnO_4$ at 10 K possess lower values than those at 300 K. With decreasing ionic size the magnitudes of cell parameters (*a*, *c*, and cell volume) tend to be reduced. By the inspection of a relation between the cell parameters and the mean radii $\langle r \rangle$ of the rare-earth ions with nine coordination based on Shannon's ionic radius table,[19] we have found an interesting anisotropic behavior. The *c* axis decreases by ∼0.31% while the *a* axis lies in ∼0.55% reduction, when the unit cell parameters of $La_{0.5}Sr_{1.5}MnO_4$ are compared with those of $Nd_{0.5}Sr_{1.5}MnO_4$. As shown in Figure 3, the $[MnO_6]$ octahedra are connected via corner-shared oxygen to form two-dimensional layers in the *ab* plane. It is thus natural to expect that the axes react anisotropically to the applied perturbation.

The temperature dependence of cell parameters for $Nd_{0.5}Sr_{1.5}MnO_4$ is shown in Figure 4. With decreasing temperatures, the overall feature can be visualized as

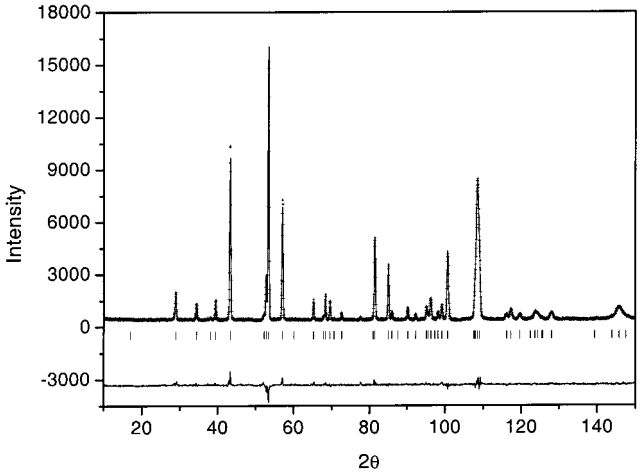

Figure 1. Observed, calculated, and difference neutron diffraction patterns for $Nd_{0.5}Sr_{1.5}MnO_4$ at 300 K. The difference between the observed and calculated patterns is displayed at the bottom of figure. Vertical bars indicate the expected reflection positions.

(17) Moritomo, Y.; Nakamura, A.; Mori, S.; Yamamoto, N.; Ohoyama, K.; Ohashi, M. *Phys. Rev.* **1997**, *B56*, 14879.

(18) Roisnel, T.; Rodríguez-Carvajal, J. *Program: Fullprof*; LLB-LCSIM: France, 2000.

(19) Shannon, R. D. *Acta Crystallogr.* **1976**, *A32*, 751.

Table 1. Refined Structural Parameters from Neutron Powder Diffraction Data for $R_{0.5}Sr_{1.5}MnO_4$[a]

parameter	R = La		R = Pr		R = Nd	
temperature	10 K	300 K	10 K	300 K	10 K	300 K
a (Å)	3.8532(1)	3.8611(1)	3.8362(1)	3.8440(1)	3.8311(1)	3.8398(1)
c (Å)	12.4055(3)	12.4258(6)	12.3950(2)	12.4103(2)	12.3685(2)	12.3878(2)
V (Å^3)	184.19(1)	185.24(1)	182.41(1)	183.38(2)	181.54(1)	182.65(1)
R/Sr B_{iso} (Å^2)	0.04(3)	0.31(4)	0.16(2)	0.29(2)	0.05(2)	0.20(2)
z	0.3580(1)	0.3582(1)	0.3574(1)	0.3575(1)	0.3578(1)	0.3578(1)
Mn B_{iso} (Å^2)	0.19(7)	0.36(8)	0.04(4)	0.19(5)	0.05(4)	0.15(5)
O1 B_{iso} (Å^2)	0.55(4)	0.77(4)	0.40(2)	0.61(3)	0.44(2)	0.68(3)
O2 B_{iso} (Å^2)	0.57(4)	0.90(5)	0.70(3)	0.97(3)	0.71(3)	1.02(3)
z	0.1615(2)	0.1613(2)	0.1624(1)	0.1623(1)	0.1623(1)	0.1623(1)
R_p (%)	6.33	6.26	4.86	4.88	4.07	4.58
R_{wp} (%)	8.12	7.83	6.21	6.09	5.34	5.87
χ^2	2.88	2.73	2.46	2.47	3.67	2.32

[a] Space group $I4/mmm$. The atomic positions are R/Sr, 4*e* (0,0,*z*); Mn, 2a (0,0,0); O1, 4*c* (0,0.5,0); O2, 4*e*(0,0,*z*).

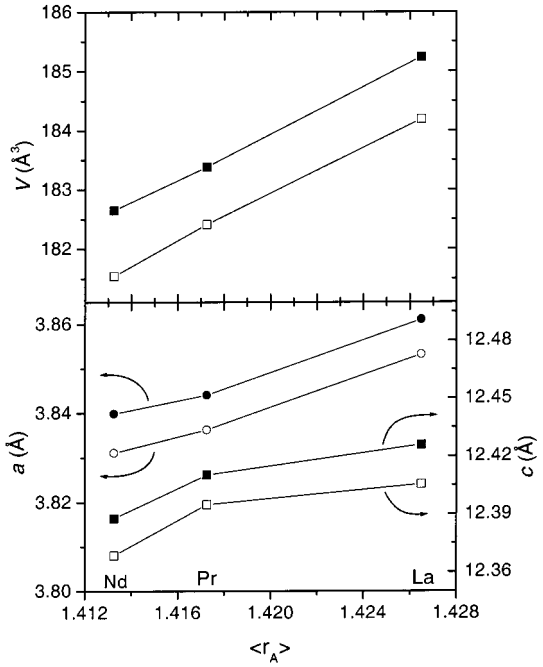

Figure 2. Variation of unit cell volume (top) and *a* and *c* axes (bottom) as a function of mean radius of A site ions at 300 and 10 K. Open and filled symbols represent the data at 10 and 300 K, respectively.

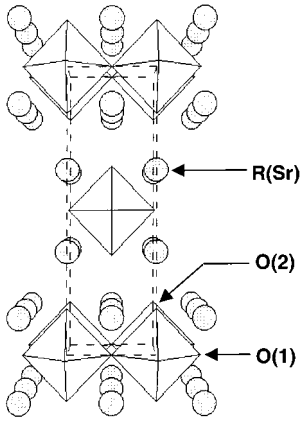

Figure 3. Crystal structure of $R_{0.5}Sr_{1.5}MnO_4$ (R = La, Pr, and Nd). Shaded circles represent the positions for R(Sr). The octahedron consists of six oxygen atoms and a Mn atom that resides in the center of the octahedron.

the gradual reduction. However, there are noticeable changes in the *a* and *c* parameters in the low-temperature regime. The *a* axis is monotonically reduced down

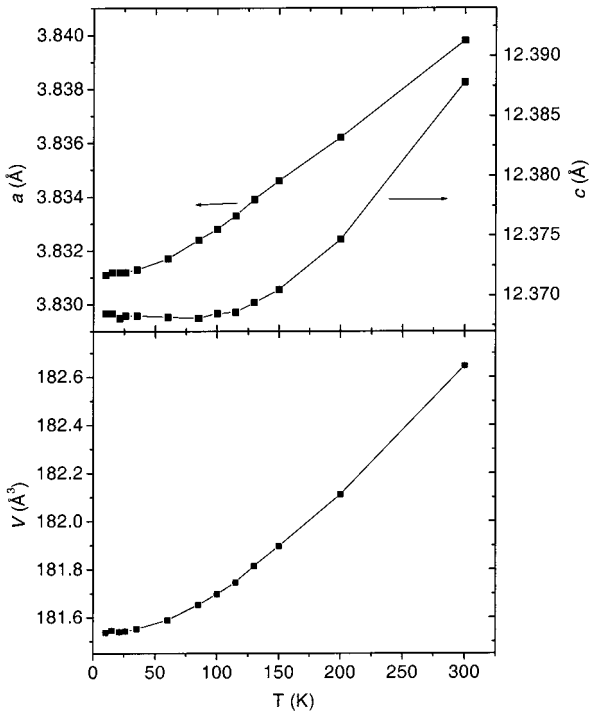

Figure 4. Temperature dependence of *a* and *c* axes for $Nd_{0.5}Sr_{1.5}MnO_4$ (top) and corresponding variation of unit cell volume (bottom).

to 85 K, but there is a curvature at around 60 K. Below 25 K, no virtual contraction is noticed. A similar trend is found in the *c* axis where a curvature occurs at about 130 K and a plateau is formed below 110 K. The contractions of the *a* and *c* axes over the structural variation amount to ~0.23% and ~0.16%, respectively. This anisotropic behavior is expected from the result of the substitution effect of the rare-earth metal ions as seen in Figure 2. The unit cell volume decreases gradually and then encounters a plateau below 35 K with the overall contraction of ~0.6%.

The temperature dependence of HRPD data for $Nd_{0.5}Sr_{1.5}MnO_4$ is shown in the left panel of Figure 5. A noticeable feature is that the superlattice peaks at around $2\theta = 14°$, 22°, 26°, and 31°, in addition to nuclear reflections, begin to grow at about 130 K. The peaks can be indexed using a magnetically ordered $2\sqrt{2}a \times 2\sqrt{2}a \times 2c$ unit cell relative to the structural unit cell. On the basis of the neutron diffraction work on $La_{0.5}Sr_{1.5}MnO_4$ by Sternlieb et al.,[14] this signals the presence of an antiferromagnetic arrangement between Mn^{3+} and Mn^{4+}

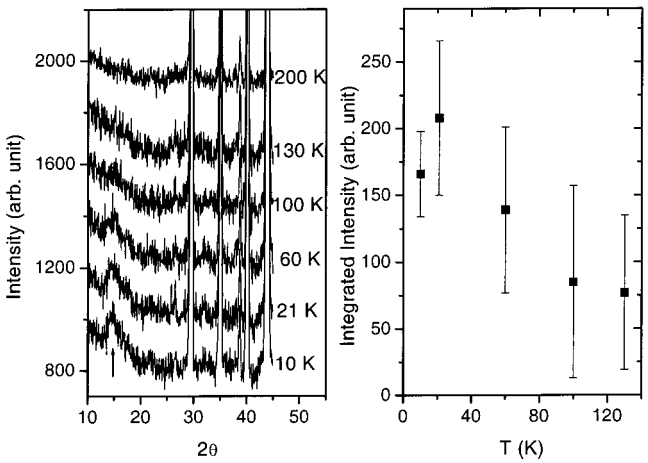

Figure 5. Temperature evolution of neutron diffraction data in the low-angle region of 2θ for $Nd_{0.5}Sr_{1.5}MnO_4$ (left) and integrated intensity of the (012) superlattice peak, marked by an up arrow in the left panel (right).

magnetic ions. The possibility of the charge ordered unit cell which has dimensions of $\sqrt{2}a \times \sqrt{2}a \times c$ can be excluded because of disparity with the observed superlattice peaks.[14] However, precise indexing of the superlattice reflections would remain elusive at this stage due to the small and broad Bragg peaks. The right panel of Figure 5 shows the integrated intensity corresponding to the (012) reflection based on the supercell unit of $2\sqrt{2}a \times 2\sqrt{2}a \times 2c$, which is the most intense superlattice reflection. The intensity appears below 130 K and gradually increases with decreasing temperature. Any discernible change in the diffraction pattern is invisible below 21 K at which, based on the magnetic data (vide post), the Nd magnetic ordering would be operative. As a result, it is conceivable that a frustrated magnetic state takes place in the Nd arrangement.

The ac magnetic susceptibility of $Nd_{0.5}Sr_{1.5}MnO_4$ was measured as a function of temperature under the conditions of a zero dc field, an ac amplitude of 10 G, and a frequency of 5 kHz, where the field direction is parallel to the *ab* plane. The top panel in Figure 6 shows the real part (χ') of ac susceptibility. With decreasing temperature, the χ' value is increased in the high-temperature region, which is consistent with the temperature-dependent dc magnetic susceptibility data (χ) that obeys the Curie−Weiss law in the temperature 280−360 K. The Weiss constant calculated from the dc magnetization data is 96 K, which is close to the values reported on the $La_{1-x}Sr_{1+x}MnO_4$ materials.[12] At around 130 K, the χ' value begins to deviate from linearity and exhibit a curvature which is marked with an arrow. The deviating behavior in the χ'(T) curve is probably associated with the advent of an antiferromagnetic interaction between Mn ions, which coincides with the onset of the superlattice peaks in the neutron diffraction data.

Another interesting feature in the χ'(T) curve is the occurrence of a cusp at 21 K which is also denoted as an arrow mark. The cusp of the χ'(T) curve coincides with a maximum value in the χ''(T) curve, which also occurs at about 21 K. Consequently, the phase delay of magnetization about the oscillating field becomes apparent below 21 K due to the energy loss, which arises from the magnetic ordering of Nd ions.[20,21] This explanation is manifested by the magnetization data on the $La_{0.5}Sr_{1.5}MnO_4$ compound that comprises the nonmagnetic La ion in its structure. An abrupt jump in the low-temperature region is clearly absent in the χ''(T) curve of $La_{0.5}Sr_{1.5}MnO_4$ shown in the inset of the bottom panel of Figure 6, also evidencing that an upturn at 21 K in $Nd_{0.5}Sr_{1.5}MnO_4$ is ascribed to the Nd magnetic ordering (T_{Nd}). To unravel the magnetic nature of the Nd ordering at 21 K, the temperature dependence of χ' was recorded at frequencies of 100, 1000, and 5000 Hz, which is shown in the inset of the top panel of Figure 6. The observation of the frequency dependence below 21 K suggests the existence of a magnetic frustration among the Nd spins.

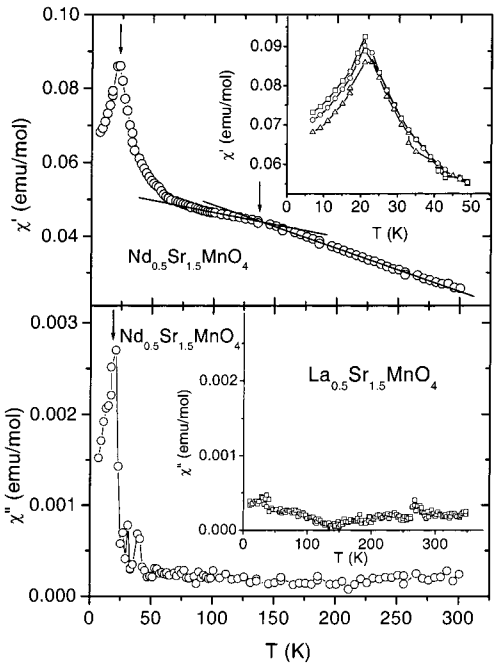

Figure 6. Real, χ' (top), and imaginary, χ'' (bottom), parts of ac magnetic susceptibility for $Nd_{0.5}Sr_{1.5}MnO_4$ as a function of temperature. The conditions are as follows: zero dc field, ac amplitude of 10 G, and a frequency of 5 kHz. The applied field is parallel to the *ab* plane. The inset in the top panel represents the temperature dependence of χ' at frequencies of 100 (□), 1000 (○), and 5000 (△) Hz for $Nd_{0.5}Sr_{1.5}MnO_4$. The inset in the bottom panel shows the temperature-dependent χ'' curve for $La_{0.5}Sr_{1.5}MnO_4$. The down-arrows express the critical temperatures.

Additional evidence of the magnetic frustration is found in the dc magnetization measurement in which the divergence of FC (field-cooled) and ZFC (zero-field-cooled) magnetization data occurs below 21 K, as shown in Figure 7. This implicates that the Nd spin undergoes different types of magnetic interactions with adjacent Nd and Mn spins, resulting in the frustration of the Nd spins. Another plausible explanation for the spin glassy behavior is to take into account the disorder of Nd and Sr ions over the same sites. The former seems more conceivable since the involvement of Mn spins in the magnetic frustration may be realized in the sudden variation of the axial Mn−O(2) bond distance at 21 K

(20) Battle, P. D.; Green, M. A.; Laskey, N. S.; Millburn, J. E.; Radaelli, P. G.; Rosseinsky, M. J.; Sullivan, S. P.; Vente, J. F. *Phys. Rev.* **1996**, *B54*, 15967.
(21) Sundaresan, A.; Caignaert, V.; Maignan, A.; Raveau, B. *Phys. Rev.* **1999**, *B60*, 533.

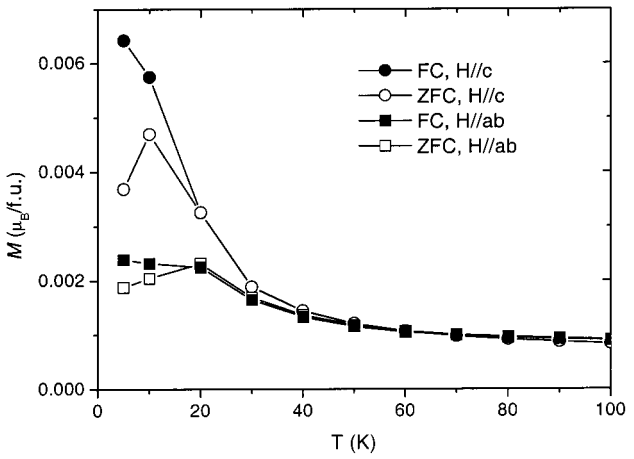

Figure 7. Temperature dependence of FC and ZFC magnetization data at 100 G for $Nd_{0.5}Sr_{1.5}MnO_4$ with different crystal orientations.

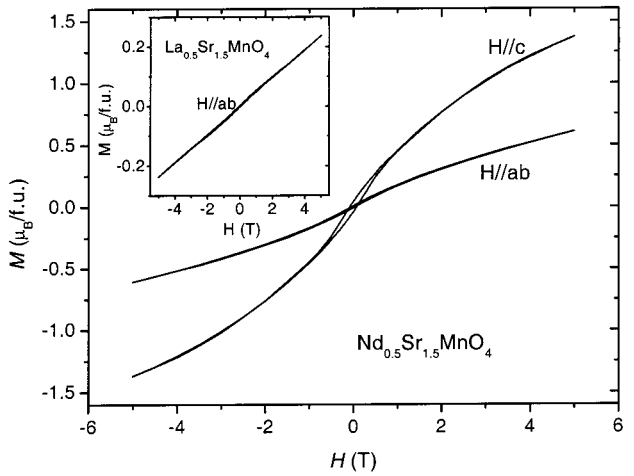

Figure 8. Field dependence of the magnetization at 5 K for $Nd_{0.5}Sr_{1.5}MnO_4$. The inset shows the field dependence of the magnetization at 5 K of $La_{0.5}Sr_{1.5}MnO_4$.

that will be discussed below. Another interesting point in Figure 7 is that the magnetization value along the *c* axis is larger than that in the *ab* plane, designating that the Nd spins are located closer to the *c* axis. This result is also established by the field dependence of magnetization at 5 K as seen in Figure 8. The larger magnetization values are seen along the *c* axis in the whole field range. The *c*-axis magnetization value is 1.37 μ_B at 5 T, which is smaller than the saturated value of Nd ion (1.64 μ_B) but much higher than that in the *ab* plane (0.61 μ_B). The effect of Nd spins, albeit small, remains in the *ab* plane since all magnetization values in the isostructural $La_{0.5}Sr_{1.5}MnO_4$ are smaller than those in $Nd_{0.5}Sr_{1.5}MnO_4$ in the *ab* plane, as displayed in the inset of Figure 8. In $Nd_{0.5}Sr_{1.5}MnO_4$, there are hysteresis behaviors in which coercive fields of the *c* axis and the *ab* plane are 800 and 400 G, respectively. This is due to the glassy state in the Nd magnetic spins.

To understand the magnetic correlation with the structure in $Nd_{0.5}Sr_{1.5}MnO_4$, we have examined the variation of bond distances with temperature. Table 2 summarizes selected bond lengths for $R_{0.5}Sr_{1.5}MnO_4$. With decreasing the size of the rare-earth ion, equatorial Mn−O(1) bond is compressed while the axial Mn−O(2) bond tends to increase. This leads to the enhancement of Jahn−Teller distortion value $D = d_{Mn-O(ax)}/d_{Mn-O(eq)}$

Table 2. Selected Bond Lengths (Å) in $R_{0.5}Sr_{1.5}MnO_4$

temperature	10 K	300 K
	R = La	
La(Sr)−O1	2.6102(9) × 4	2.6138(10) × 4
La(Sr)−O2	2.4379(23)	2.4468(25)
La(Sr)−O2	2.7354(2) × 4	2.7409(2) × 4
Mn−O1	1.9266 × 4	1.9306 × 4
Mn−O2	2.0037(17) × 2	2.0040(27) × 2
	R = Pr	
Pr(Sr)−O1	2.6081(7) × 4	2.6120(8) × 4
Pr(Sr)−O2	2.4177(16)	2.4224(18)
Pr(Sr)−O2	2.7237(1) × 4	2.7291(2) × 4
Mn−O1	1.9181 × 4	1.9220 × 4
Mn−O2	2.0126(10) × 2	2.0141(27) × 2
	R = Nd	
Nd(Sr)−O1	2.6001(6) × 4	2.6053(7) × 4
Nd(Sr)−O2	2.4180(14)	2.4226(17)
Nd(Sr)−O2	2.7205(1) × 4	2.7266(2) × 4
Mn−O1	1.9155 × 4	1.9199 × 4
Mn−O2	2.0080(9) × 2	2.0102(11) × 2

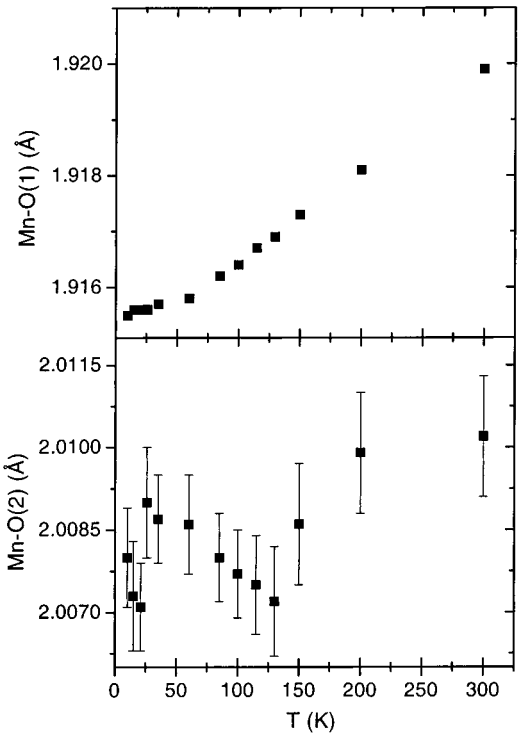

Figure 9. Temperature dependence of Mn−O(1) (top) and Mn−O(2) (bottom) bond lengths for $Nd_{0.5}Sr_{1.5}MnO_4$.

from 1.04 for R = La to 1.05 for R = Pr and Nd. Here, $d_{Mn-O(ax)}$ is the distance between Mn and axial oxygen, and $d_{Mn-O(eq)}$ is between Mn and equatorial oxygen atom. As can be seen in Figure 3, there are two crystallographically distinctive oxygen sites in its structure. One denoted as O(1) is located at the equatorial position of the [MnO_6] octahedron and the other, O(2), lies in the axial position. The axial Mn−O(2) bond distance is slightly longer than the equatorial Mn−O(1) one in the entire temperature region, as shown in Figure 9. As anticipated from the structure, the temperature dependence of the Mn−O(1) bond length is quite similar to the *a* axis variation illustrated in Figure 4. On the other hand, the change of the Mn−O(2) bond with temperature does not directly reflect the variation of the *c* axis. With decreasing temperature, the Mn−O(2) bond distance appears to be gradually reduced but reaches a local minimum at 130 K that corresponds to

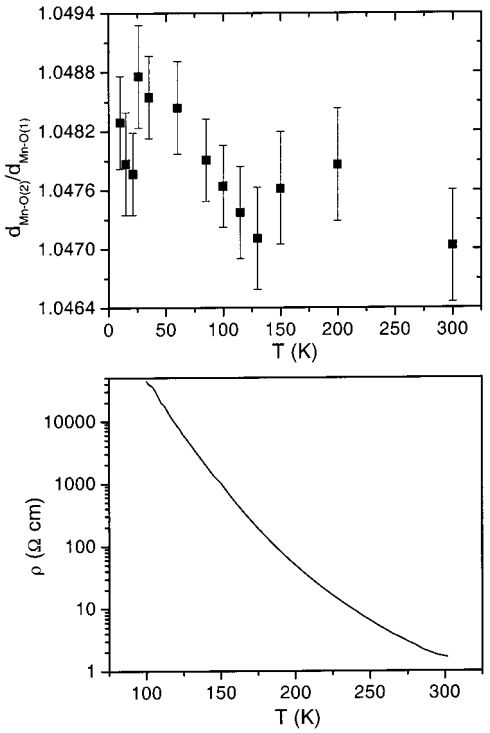

Figure 10. Temperature dependence of the Jahn−Teller distortion (*D*) value (top) and the in-plane resistivity (bottom) for $Nd_{0.5}Sr_{1.5}MnO_4$.

the onsets of the superlattice diffraction peaks on the neutron diffraction data and the antiferromagnetic transition in the ac susceptibility data. Below 130 K, the Mn−O(2) bond distance is slightly increased with decreasing temperature but undergoes a drastic drop at 21 K. This is accompanied by the abrupt change in the magnetic data as shown in Figure 6, indicating the association of the Nd magnetic ordering. It is worthy to note that the structural changes at T_N and T_{Nd} track the magnetic variation, as seen in Figure 6. Our results on $Nd_{0.5}Sr_{1.5}MnO_4$ suggest that the Mn−O(2) bond along the *c* axis is more strongly correlated with the magnetic transition than the equatorial component in the *ab* plane.

The top panel of Figure 10 represents the temperature dependence of Jahn−Teller distortion (*D*) for $Nd_{0.5}Sr_{1.5}MnO_4$. Interestingly, the *D* value is gradually increased below 130 K. This implicates that the enlarged structural distortion in the low-temperature regime renders itinerant electrons localized and produces an insulating state, which is verified by the resistivity curve in the *ab* plane as shown in the bottom panel of Figure 10. Any noticeable anomaly in the resistivity curve is not observed in $Nd_{0.5}Sr_{1.5}MnO_4$. This is quite different from that found in the $La_{0.5}Sr_{1.5}MnO_4$ system at the same doping level,[12] in which an abrupt increase of the resistivity curve occurs at a charge-ordering temperature. This suggests that charge ordering is unlikely to be involved in $Nd_{0.5}Sr_{1.5}MnO_4$,[17] which is in accord with the neutron diffraction result. Another concomitant noteworthy feature in Figure 10 is that a sudden drop of *D* is aroused at $T_{Nd} = 21$ K. From these results, it is evident that the variation of the Mn−O(2) bond is strongly correlated with the magnetic transition since the abrupt changes of *D* occur in the vicinity of T_N and T_{Nd}.

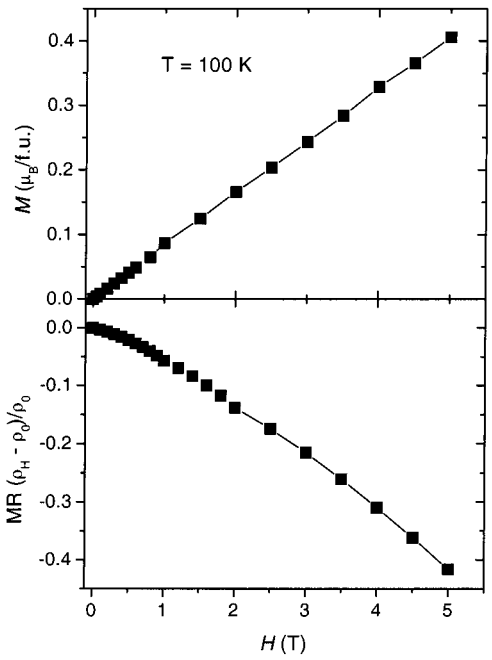

Figure 11. Field dependence of the magnetization (top) and the magneto resistance (bottom) at 100 K for $Nd_{0.5}Sr_{1.5}MnO_4$.

Figure 11 shows the field dependence of magnetization and magneto resistance (MR) for $Nd_{0.5}Sr_{1.5}MnO_4$ at 100 K in which MR is defined as $(\rho_H - \rho_0)/\rho_0$. Here, ρ_0 stands for the resistivity at zero magnetic field and ρ_H at a certain field. The application of a magnetic field causes a monotonic rise of magnetization at 100 K. The negative MR value reaches 42% at 5 T. This observation demonstrates that locally confined itinerant electrons hop easily between Mn sites, which is favored by field-induced enhanced spin alignment.[22]

Conclusions

We have investigated magnetic and structural properties on single crystals of $R_{0.5}Sr_{1.5}MnO_4$ (R = La, Pr, and Nd). In particular, we put emphasis on the structure and its correlation with the magnetic properties of $Nd_{0.5}Sr_{1.5}MnO_4$. An important finding in the $Nd_{0.5}Sr_{1.5}MnO_4$ system is that the structural variation is strongly correlated with the magnetic transition. The data presented here reveal that $Nd_{0.5}Sr_{1.5}MnO_4$ has two magnetic transitions at $T_N \approx 130$ K and $T_{Nd} \approx 21$ K. The first transition at 130 K appears to be associated with the antiferromagnetic ordering, which is evidenced by superlattice peaks in the neutron diffraction pattern of $Nd_{0.5}Sr_{1.5}MnO_4$. The second one at 21 K is ascribed to the Nd ordering, which is verified by the direct comparison of the $\chi''(T)$ plot between $Nd_{0.5}Sr_{1.5}MnO_4$ and $La_{0.5}Sr_{1.5}MnO_4$. The Nd ordering exhibits spin glasslike behavior. This is presumably due to the competition between Nd−Nd and Nd−Mn magnetic interactions. Another interesting feature in $Nd_{0.5}Sr_{1.5}MnO_4$ is that the lattice component along the *c* axis directly reflects the magnetic arrangement. With decreasing temperatures, the axial Mn−O(2) bond distance is more dramatically varied than the equatorial one. It is intriguing to note that the axial bond and the Jahn−

(22) Kimura, T.; Kumai, R.; Tokura, Y.; Li, J. Q.; Matsui, Y. *Phys. Rev.* **1998**, *B58*, 11081.

Teller distortion exhibit local anomalies at specific temperatures that coincide with the occurrence of magnetic orderings. From our structural and magnetization measurements, we conclude that the magnetic correlations originated from interacting Mn ions or Nd ions are strongly coupled with the structural variation in $Nd_{0.5}Sr_{1.5}MnO_4$.

Acknowledgment. We are grateful to J. S. Shin, H. S. Choi, J. H. Dho for kind cooperation and helpful discussion. We also acknowledge J. G. Park for his valuable comments on our work. The Creative Research Initiative Program financially sponsored this work.

CM000702N